Article

Numerical Simulation of Frost Heave Deformation of Concrete-Lined Canal Considering Thermal-Hydro-Mechanical Coupling Effect

Renjie Teng, Xin Gu (ID) **, Xiaozhou Xia and Qing Zhang ***

College of Mechanics and Materials, Hohai University, Nanjing 211100, China
* Correspondence: lxzhangqing@hhu.edu.cn

Abstract: This work presents a comprehensive coupled thermal-hydro-mechanical model to explore the frost heave mechanism of the concrete-lined canal under a freeze–thaw environment. Unlike previous models that regard concrete as a homogeneous material, this model considers concrete a porous medium and considers the effect of the concrete pore structure, as well as the water content, ice content, and ice-water phase transition, on the mechanical deformation of the canal. Firstly, based on the theories of unsaturated soil mechanics, thermodynamics, and poroelasticity, the thermal-hydro-mechanical coupling equations of the soil under the freeze–thaw condition are established. Then, based on the theories of thermodynamics, poroelasticity, and permeability mechanics of porous media, the thermal-hydro-mechanical coupling equations of the concrete under the freeze–thaw condition are established. Finally, the freeze–thaw simulation of a canal is carried out and compared with the referred indoor model test, in which the evolution behavior of temperature, frost depth, and frost heave deformation of the canal are studied. The results show that the freezing process of the soil foundation is a unidirectional process that develops from the surface to the bottom, and the thawing process of the soil foundation is a bidirectional process that thaws from the surface and bottom to the center. The frost heave deformation of the soil foundation at the 1/2~1/3 slope height area is the largest, which may easily lead to frost heave damage to the concrete lining in this area. The frost heave deformation of the canal obtained by the numerical simulation is consistent with the experimental results, which illustrates the validity of the established model for predicting the frost heave deformation of concrete-lined canals.

Keywords: concrete-lined canal; thermal-hydro-mechanical coupling; frost heave deformation

1. Introduction

In cold and arid regions, the concrete-lined canal is widely used in water conveyance and agricultural irrigation, such as the South-to-North Water Transfer Project in China [1] and the State Water Project in California [2]. Under the freeze–thaw environment, the freezing and thawing of the soil usually cause uneven deformation of the soil foundation, thus causing damage to the canal, such as the lining cracking and surface heaving. According to statistics, in China, 50–60% of the canals in Qinghai Province suffered serious frost heave damage [3]. Over 90 canals in a large irrigation district in Heilongjiang Province were damaged by frost heaving, accounting for 83% of the total canals [4]. The frost heave damage not only limits the water conveyance capacity of the canal but also increases the maintenance cost. To reduce the damage caused by frost heave deformation, it is important to conduct in-depth research on the frost heave mechanism of the concrete-lined canal.

Scholars have carried out extensive research on the frost heave mechanism of the soil by experimental method. Taber [5] experimentally observed the phenomenon of moisture migration and water freezing during the freeze–thaw process of soil and pointed out that water migration and ice-water phase transition are the main reasons for the frost heave

deformation of soil. Through comparative studies, Taber concluded that soil composition, water content, and freezing rate are the main factors affecting the frost heave deformation of soil. Everett [6] quantitatively analyzed the frost heave deformation and frost heave force through experiments and proposed the so-called capillary theory from the point of view of equilibrium thermodynamics. The migration of unfrozen water in capillary caused by frost heave force and suction force is the main reason for developing the frost heave deformation of soil. Although the capillary theory can better describe the evolution of the frost heave deformation of the soil, the calculated results obtained by this theory are quite different from the experimental data. Miller [7] explored the reason for this discrepancy and proposed the so-called frozen fringe theory. During the freezing process of the soil, there is a non-freezing water area with low moisture content and low thermal conductivity between the frozen and the unfrozen area. The fluidity and hydraulic pressure of this non-freezing water play a decisive role in the moisture migration and the frost heave deformation of the soil. With the continuous development of experimental technology, the study of soil frost heaves has gradually transformed from a single physical field problem to a thermal-hydro-mechanical coupled one, reflecting the water migration, heat transfer, ice-water phase transition, and structural constraints. Scholars have established various models to predict the frost heave characteristics of soil, such as the rigid ice model and the hydrodynamic model. Based on the frozen fringe theory, O'Neill [8] established a thermal-hydro coupled soil model under freeze–thaw conditions (the so-called rigid ice model). The rigid ice model comprehensively considers various factors (migration velocity of pore water, pore pressure, ice crystal formation rate, etc.), so the governing equations of the model are very complex. It is generally necessary to simplify the model in numerical calculations. Harlan [9] experimentally pointed out that frost heave deformation occurs only when the ice content of the soil exceeds a certain value during the freezing process. Based on mass conservation and energy conservation, he established the thermal-hydro coupled model of soil under freeze–thaw conditions (the so-called hydrodynamic model). The moisture migration and the frost heave deformation of the soil can be described by the distribution of the moisture and temperature. Compared with the rigid ice model, the governing equations of the hydrodynamic model are more concise and intuitive.

Based on the above research, some scholars have researched the frost heave problem of canals in cold regions. Mo [10] established a thermal-hydro coupled model based on the balance equations of energy and mass and pointed out that the frost heave deformation of the soil foundation reached a maximum in the 1/3 slope height area. Liu [11] added the latent heat of phase transformation to the heat conduction equation in the form of equivalent heat capacity to explore the influence of ice-water phase transition on the temperature field and deformation field. The calculation results considering the latent heat of phase transformation are more accurate than those not considered. Based on Liu's research, Wang [12] established a thermal-hydro-mechanical coupled model through the frozen fringe theory. He used the finite-element method to simulate the displacement and stress fields of 30 lined canals with different sizes, revealing the size effect of lining frost heave damage. The aforementioned studies have achieved fruitful results. However, most current research on the frost heave mechanism of concrete-lined canals regards concrete as a homogeneous material. It only considers the effect of the freeze–thaw process on the soil foundation while ignoring that concrete is a porous medium and will be affected by freeze–thaw cycles.

As a complex porous medium, concrete contains a large amount of pore water. The freeze–thaw cycle causes the repeated freezing and thawing of the pore water, thus weakening the strength of concrete and making it more prone to damage [13–16]. In addition, the crack propagation during the concrete failure process is also closely related to the pore structure of the concrete [17–20]. Therefore, the effect of the freeze–thaw process on concrete needs to be involved when conducting an in-depth study of the freeze–thaw of concrete-lined canals. Scholars have carried out a lot of research on the freeze–thaw mechanism and numerical model. Powers [21] explored the freezing mechanism of concrete from the

perspective of internal pore microstructure and proposed the so-called hydraulic pressure theory. The hydraulic pressure is regarded as the main cause of concrete freezing damage, and it is generated by the water migration driven by the freezing of pore water. Based on the porosity of cement-based materials, Coussy [22,23] studied the physical process of ice crystal growth in the concrete pores and derived the poroelastic constitutive equations of the concrete during the freeze–thaw process, which provided a new perspective on the computation of the stress and strain during the freeze–thaw process of concrete. Based on the porosity mechanics, the hydraulic pressure theory, and the local thermodynamic equilibrium between various phases, Zuber [24,25] established the thermal-hydro coupling equations of concrete under freeze–thaw conditions, respectively, for mass conservation, momentum conservation, and energy conservation. Duan [26] developed and established the thermal-hydro-mechanical coupling model of the concrete under freeze–thaw conditions based on the model developed by Zuber and pointed out that the heat conduction of the concrete during the freeze–thaw process was related to the frost heave deformation and the moisture migration. Through finite-element analysis, he obtained the development of stress and strain of the concrete column specimens. Pan [27] experimentally measured the pore size distribution curve of concrete and conducted a numerical simulation through Zuber's thermal-hydro coupling equation to explore the influence of porosity and pore size distribution on the freeze–thaw behavior of concrete. The above researches provide modeling ideas and relatively complete governing equations for the study of concrete under freeze–thaw conditions, which can greatly support the present modeling of the concrete lining during the freeze–thaw process of the concrete-lined canal.

This study aims to establish a comprehensive calculation model to explore the frost heave mechanisms of canals under freeze–thaw conditions. Firstly, based on unsaturated soil mechanics, thermodynamics, and poroelasticity, the thermal-hydro-mechanical coupling equations of the soil under the freeze–thaw condition are established. Next, considering the influence of the pore structure of concrete, the thermal-hydro-mechanical coupling equations of the concrete under the freeze–thaw environment are established based on the thermodynamics, poroelasticity, and permeability mechanics of porous media. Then, the evolution of temperature, frost depth, and frost heave deformation of the canal are analyzed by using the finite element method. Then the simulation results and the experimental results are compared to demonstrate the established model. Finally, the development process of frost heave deformation of the soil foundation is summarized, and the easily frost-damaged zone of the canal is pointed out according to the distribution of frost heave deformation. Overall, regarding concrete as a porous medium and considering the influence of the pore structure of concrete, this paper presents a new calculation model for the concrete-lined canal under a freeze–thaw environment, in which both the thermodynamic performance of concrete and soil during the freeze–thaw process can be reflected. As a preliminary study, the numerical model and results in this study can give a reference for the design and protection of concrete-lined canals and provide a new idea for analyzing frost heave failure.

2. Multi-Physics Coupling Equations of Soil

2.1. Seepage Field

Based on Richard's equation and the mass conservation of ice and water under freeze–thaw conditions, considering the hindering effect of the icing of pore water on the migration of unfrozen water [28], the migration equation of unfrozen water in the soil during the freeze–thaw process can be expressed as:

$$\frac{\partial \theta_w}{\partial t} + \frac{\rho_i}{\rho_w}\left(\frac{\partial \theta_i}{\partial t}\right) = \nabla \cdot [D(\theta_w)\nabla\theta_w + k_g(\theta_w)], \tag{1}$$

where θ_w and θ_i are the volume content of water and ice in the soil, respectively, ρ_i and ρ_w are the mass density of ice and water, respectively, $k_g(\theta_w)$ represents the moisture migration

caused by gravity and is negligible in the freeze–thaw problem. $D(\theta_w)$ represents the diffusion coefficient of water in the soil, expressed as [28]:

$$D(\theta_w) = \left(\frac{k(\theta_w)}{c(\theta_w)}\right) I(\theta_w), \tag{2}$$

where $k(\theta_w)$, $c(\theta_w)$ and $I(\theta_w)$ represent the hydraulic conductivity of soil, the specific gravity of water, and the ice impedance factor, respectively.

2.2. Temperature Field

The heat conduction of soil during the freeze–thaw process follows Fourier's law. Considering the effect of the water content and ice content on the heat conduction of soil and regarding the soil as a system composed of water, ice, and soil, the thermodynamic equilibrium equation of soil, including the ice-water phase transition, can be expressed as [29]:

$$\begin{cases} \rho C \frac{\partial T}{\partial t} = \nabla \cdot (\lambda \nabla T) + L\rho_i \frac{\partial \theta_i}{\partial t} \\ \rho C = \rho_w \theta_w C_w + \rho_i \theta_i C_i + \rho_s(1-\theta_s)C_s \\ \lambda = \theta_w \lambda_w + \theta_i \lambda_i + (1-\theta_s)\lambda_s \end{cases}, \tag{3}$$

where ρ is the mass density of the system, T is the current temperature, L is the latent heat of water, C, C_w, C_i and C_s are the heat capacities of system, water, ice, and soil, respectively, θ_s is the volume content of water at saturation, ρ_s is the mass density of soil, λ, λ_w, λ_i and λ_s are the thermal conductivities of system, water, ice, and soil, respectively.

2.3. Dynamic Equilibrium Relationship of Ice-Water Phase Transition

The water begins to freeze when the temperature of the soil is lower than its freezing point. Through experimental research and considering the mass conservation of the water and ice in the soil, the dynamic equilibrium relationship between ice content, water content, and temperature during the freeze–thaw process can be expressed in the following form [30]:

$$B(T) = \frac{\theta_i}{\theta_w} = \begin{cases} \frac{\rho_w}{\rho_i}\left(\frac{T}{T_f}\right)^A - 1 & T < T_f \\ 0 & T \geq T_f \end{cases}, \tag{4}$$

$$\theta_i = B(T)\theta_w$$

where $B(T)$ is the solid-liquid ratio, i.e., the ratio between the volume content of ice and the volume content of water, T_f is the freezing point of water, A is a constant related to soil properties, e.g., $A = 0.56$ for the silty clay.

Equation (4) reflects the dynamic equilibrium relationship of ice content, water content, and temperature during the freeze–thaw process of the soil. Under the given temperature conditions, the temperature field and seepage field of the soil during the freeze–thaw process can be solved by the simultaneous equations composed of Equations (1), (3), and (4), and then the ice content distribution of the soil can be obtained for stress analysis.

2.4. Stress Field

In this paper, the hydrodynamic model is used to calculate the frost heave deformation of soil. The hydrodynamic model is believed that when the mass fraction of ice in the soil exceeds a certain critical value, the frost heave deformation of the soil begins to occur.

Assuming that the frost heave of the soil is an isotropic volume expansion, the corresponding frost heave coefficient can be determined from the ice content distribution during the frost heave process of soil. For silty clay, the functional relationship between the frost heave coefficient and the ice content can be taken as [30,31]:

$$\eta(\omega_{\theta_i}) = \begin{cases} 0.089\omega_{\theta_i} - 0.0003 & \omega_{\theta_i} > 0.003 \\ 0 & \omega_{\theta_i} < 0.003 \end{cases}, \tag{5}$$

where $\eta(\omega_{\theta_i})$ is the frost heave coefficient, ω_{θ_i} represents the mass fraction of ice, i.e., $\omega_{\theta_i} = \rho_i \theta_i / \rho_s$.

The frost heave strain tensor of soil can be obtained as:

$$\boldsymbol{\varepsilon_f} = \eta(\omega_{\theta_i})\,\mathbf{I}, \tag{6}$$

where $\boldsymbol{\varepsilon_f}$ is the frost heave strain tensor of soil and $\mathbf{I}$ is the second-order identity tensor.

The general equation of mechanical equilibrium of porous materials under freeze–thaw conditions can be expressed as:

$$\nabla \cdot \boldsymbol{\sigma} + \mathbf{F} = \mathbf{0}, \tag{7}$$

where $\boldsymbol{\sigma}$ is the total stress tensor, $\mathbf{F}$ is the vector of body force density.

From Equations (5)–(7), the governing equation of the stress field of soil under freeze–thaw conditions can be expressed as:

$$\nabla \cdot \left[\mathbf{H_s} : (\boldsymbol{\varepsilon_s} - \eta(\omega_{\theta_i})\mathbf{I}) \right] + \mathbf{F_s} = \mathbf{0}, \tag{8}$$

where $\mathbf{H_s}$ is the elastic tensor of soil, $\boldsymbol{\varepsilon_s}$ is the total strain tensor of soil, and $\mathbf{F_s}$ is the vector of body force density of soil.

As stated previously, the thermal-hydro-mechanical coupling equations of the soil under freeze–thaw conditions are made up of three sorts, i.e., the mass conservation equation, which contains the influences of water migration and ice formation; the energy conservation equation of the coupling between ice-water phase transition and heat transfer; the mechanical equilibrium equation which takes into the effect of frost heave deformation. The unknowns of the coupled equations are temperature, ice content, and displacement. The temperature field and seepage field are bidirectionally coupled, and the stress field is unidirectionally coupled with them through the ice content.

3. Multi-Physics Coupling Equations of Concrete

The thermal-hydro-mechanical coupling equations considering the pore structure of concrete are established, which can reflect the thermodynamic properties of concrete under freeze–thaw conditions and lay the foundation for research on the damage and cracking of concrete lining in the future.

3.1. Stress Field

Regarding concrete as an elastic porous medium, concrete is composed of water, ice, and skeleton under freeze–thaw conditions. According to the principle of effective stress, the total stress of concrete is composed of two parts, i.e., skeleton stress and pore pressure [24]:

$$\boldsymbol{\sigma_c} = \boldsymbol{\sigma}' - b p^* \mathbf{I}, \tag{9}$$

where $\boldsymbol{\sigma_c}$ is the total stress tensor of concrete, $\boldsymbol{\sigma}'$ is the effective stress tensor, i.e., the stress tensor governing the skeleton deformation, $\mathbf{I}$ is the second-order identity tensor, p^* is the mean pressure exerted on the pore walls. $b = 1 - K_c / K_m$ is Biot's coefficient, where K_c and K_m are the compressibility moduli of the concrete and the skeleton, respectively.

During the freeze–thaw process, the total strain of concrete consists of the thermal and elastic strain. Therefore, the elastic constitutive relationship between effective stress and strain can be expressed as:

$$\begin{aligned} \boldsymbol{\sigma}' &= \mathbf{H_c} : \boldsymbol{\varepsilon_e} = \mathbf{H} : (\boldsymbol{\varepsilon_c} - \boldsymbol{\varepsilon_t}) \\ \boldsymbol{\varepsilon_t} &= \tfrac{1}{3}\alpha(T - T_{ref})\,\mathbf{I} \end{aligned}, \tag{10}$$

where $\mathbf{H_c}$ is the elastic tensor of concrete, $\boldsymbol{\varepsilon_e}$ is the elastic strain tensor, $\boldsymbol{\varepsilon_c}$ is the total strain tensor of concrete, $\boldsymbol{\varepsilon_t}$ is the thermal strain tensor, T is the current temperature, and T_{ref}

is the so-called reference temperature at which the thermal strain is zero $\varepsilon_t = 0$. $\bar{\alpha}$ is the volumetric thermal expansion coefficient of concrete [26]:

$$\bar{\alpha} = n\varphi_w\alpha_w + n\varphi_i\alpha_i + (b - n)\alpha_m, \tag{11}$$

where n is the total porosity of concrete, φ_w and φ_i are the volume content of ice and water in the concrete, respectively, α_w, α_i and α_m are the volumetric thermal expansion coefficient of water, ice, and skeleton, respectively.

From Equations (7), (9), and (10), the governing equation of the stress field of concrete under freeze–thaw conditions can be expressed as:

$$\nabla \cdot \left[\mathbf{H_c} : \left(\varepsilon_{\mathbf{c}} - \frac{1}{3}\bar{\alpha}(T - T_{ref})\,\mathbf{I}\right) - bp^*\mathbf{I}\right] + \mathbf{F_c} = \mathbf{0}, \tag{12}$$

where $\mathbf{F_c}$ is the vector of the body force density of concrete.

3.2. Seepage Field

Based on Darcy's law and the mass conservation of ice and water under freeze–thaw conditions, the governing equation of the seepage field of concrete considering the influence of ice-water phase transition, ice formation, heat conduction, and water migration can be derived as [25]

$$\beta\dot{p}_w = \nabla \cdot \left(\frac{D_c}{\eta}\nabla p_w\right) + S - b\dot{\varepsilon}_v, \tag{13}$$

where p_w is the pressure of pore water, D_c is the permeability coefficient of concrete, η is the fluid viscosity of water, $\dot{\varepsilon}_v$ is the volumetric strain of concrete. β is the compressibility coefficient of concrete, stated in the following form:

$$\beta = \frac{n\varphi_w}{K_w} + \frac{n\varphi_i}{K_i} + \frac{b - n}{K_m}, \tag{14}$$

where K_w and K_i are the compressibility moduli of water and ice, respectively.

In Equation (13), S is the source of pressure and can be expressed as:

$$S = \left(\frac{1}{\rho_i} - \frac{1}{\rho_w}\right)\frac{\partial V_{w\to i}}{\partial T} + \bar{\alpha}\frac{\partial T}{\partial t} - \frac{b - n}{K_m}\frac{\partial X}{\partial T} - \frac{n\varphi_i}{K_i}\frac{\partial \kappa}{\partial T}, \tag{15}$$

where ρ_i and ρ_w are the mass density of ice and water, respectively, $V_{w\to i}$ is the volume of ice in concrete formed at temperature T, κ and X are respectively related to the curvature of the ice/adsorbed layer interface and the pore pressure of ice in the frozen pores [25].

3.3. Temperature Field

The heat conduction of the porous medium follows Fourier's law. Considering the effect of the water content and ice content on the heat conduction of concrete, the heat conduction equation of concrete, including the ice-water phase transition during the freeze–thaw conditions, can be expressed as [29]:

$$\begin{cases} \rho_c C_c \frac{\partial T}{\partial t} = \nabla \cdot (\lambda_c \nabla T) + L\rho_i \frac{\partial \varphi_i}{\partial t} \\ \lambda_c = \frac{n\varphi_w\lambda_w + n\varphi_i\lambda_i + \lambda_m}{n\varphi_w + n\varphi_i + 1} \\ C_c = \frac{n\varphi_w C_w + n\varphi_i C_i + C_m}{n\varphi_w + n\varphi_i + 1} \end{cases}, \tag{16}$$

where λ_c, λ_w, λ_i and λ_m are the thermal conductivities of concrete, water, ice, and skeleton, respectively, C_c, C_w, C_i and C_m are the heat capacities of concrete, water, ice, and skeleton, respectively. ρ_c is the mass density of concrete and L is the latent heat of the water.

Based on the preceding sections, the thermal and mechanical properties of the concrete under freeze–thaw conditions can be expressed by the thermal-hydro-mechanical coupling

equations, which consist of three sorts, i.e., the mechanical equilibrium equation containing the effect of pore pressure and thermal stress; the mass conservation equation including the influences of water migration, ice formation, heat transfer, and deformation; the energy conservation equation coupling between ice-water phase transition and heat transfer. The unknowns of the coupling equations are temperature, displacement, and pore pressure. Under the given temperature conditions, the displacement and pore pressure can be obtained by solving the temperature field, stress field, and seepage field. The stress field, temperature field, and seepage field are fully coupled.

4. Computational Model and Results Analysis

4.1. Computational Model

Taking the canal in the indoor model test [32] as the calculation object, a thermal-hydro-mechanical coupled calculation model of the concrete-lined canal under freeze–thaw conditions is established.

4.1.1. Geometry Modeling and Mesh Generation

Considering the symmetry of the trapezoidal canal, one-half of the actual canal is taken as the computational configuration, as shown in Figure 1. The upper part of the model is the concrete lining, and the lower part is the soil foundation. The four-node linear isoparametric element is used to discretize the configuration, and the corresponding finite element mesh of the canal is shown in Figure 2. The finite element program Comsol Multi-physics is used for the numerical solution.
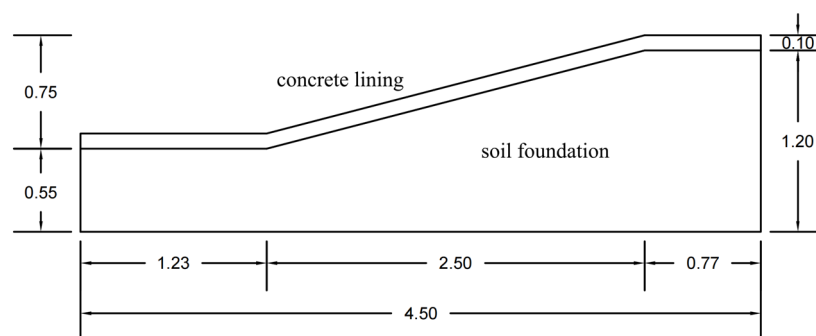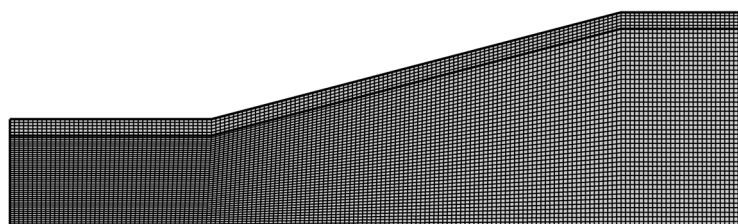

Figure 1. Geometry model of the canal (m).

Figure 2. Finite-element mesh of the canal.

4.1.2. Initial and Boundary Conditions

For the deformation (stress) field, the horizontal displacement of the left and right boundaries of the model is constrained, and the lower boundary is set as a fixed constraint.

For the temperature field, the left and right boundaries are set as adiabatic boundaries. According to the temperature setting scheme of the indoor test model, the initial temperature of the canal is set at 2 °C, and the bottom boundary is set at a constant temperature of 3 °C as a stable heat source. The upper boundary (the upper surface of the canal) is set

as the Dirichlet boundary condition, which changes with time according to the following formula:

$$T(t) = \begin{cases} 2 - \left(\frac{26}{36.4}\right)t & 0 < t < 36.4 \\ -24 & 36.4 < t < 60.8 \\ -24 + \left(\frac{44}{59.1}\right)(t - 60.8) & 60.8 < t < 119.9 \\ 20 & 119.9 < t < 160 \end{cases} \quad , \tag{17}$$

where t is the time with a unit of h. $T(t)$ is the temperature of the upper boundary, °C, it first decreases linearly from 2 °C to −24 °C, then maintains at −24 °C for some time, then linearly increases to 20 °C, and finally keeps constant at 20 °C until the end of the calculation, as is shown in Figure 3.
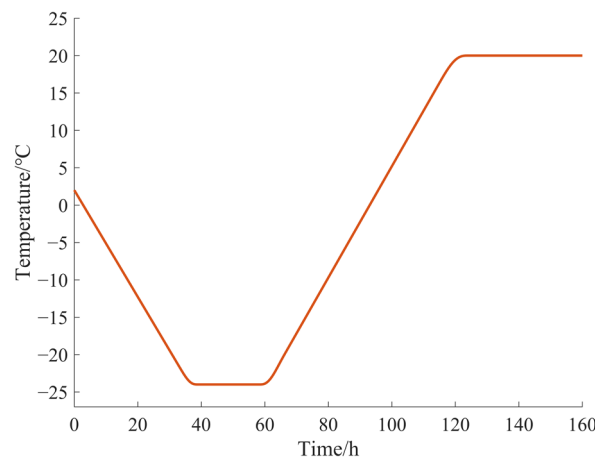
Figure 3. Temperature condition of the upper boundary (°C).

For the seepage field, the left, right, and bottom boundaries are set as no-flux boundaries. The initial water content of the soil foundation is consistent with the indoor test model, that is, the initial water content of the soil within the depth of 0~70 cm from the upper surface is set as 30%, and the initial water content of the soil within the depth of 70~120 cm is linearly reduced from 30% to 10%.

4.1.3. Calculation Parameters

The calculation parameters of the concrete lining are selected according to the values of the literature [27] and the experiment [33], as shown in Table 1. The soil parameters are consistent with the parameters of the indoor test model [32], as shown in Table 2. Table 1 also gives the necessary parameters of water and ice in the calculation.

Table 1. Calculation parameters of the concrete lining.

Composition	ρ (kg/m³)	λ (W/m·k)	C (J/kg·K)	α (GPa)	K (GPa)	E (GPa)	D (m²)	b	n
Concrete	2400	—	—	—	11.1	35	8.3×10^{-12}	0.657	0.155
Skeleton	—	1.80	950	2.0×10^{-5}	32.4	—	—	—	—
Water	1000	0.54	4200	-9.2×10^{-5}	2.0	—	—	—	—
Ice	900	2.22	2100	1.2×10^{-4}	8.0	—	—	—	—

Table 2. Calculation parameters of the soil.

Composition	ρ (kg/m³)	C (J/kg·°C)	λ (W/m·k)	T_f (°C)	E (GPa)	A
Soil	1940	1680	1.22	−0.15	0.30	0.56

The pore size distribution curve of concrete is selected from the fitting curve obtained from experiments in literature [26], that is:

$$\frac{d\phi}{dr} = a_1 + \frac{a_2}{1 + \left(\frac{r}{a_3}\right)^{a_4}}, \tag{18}$$

where $a_1 = 4.9389 \times 10^{-6}$, $a_2 = 9.366 \times 10^{-4}$, $a_3 = 9.580986 \times 10$, $a_4 = 2.27832$.

4.2. Calculation Results and Analysis

4.2.1. Evolution of Temperature Distribution

The initial temperature of the canal was 2 °C. After the calculation began, the surface temperature of the canal gradually decreased. Under the drive of the temperature gradient, the temperature of the canal gradually decreased from top to bottom, and the negative temperature developed downward continuously. The temperature distributions of the canal at the calculation time of 50 h and 80 h are given in Figure 4. The results showed that the temperature of the canal decreased in a unidirectional trend, and the drop rate of the temperature of the canal was relatively uniform.
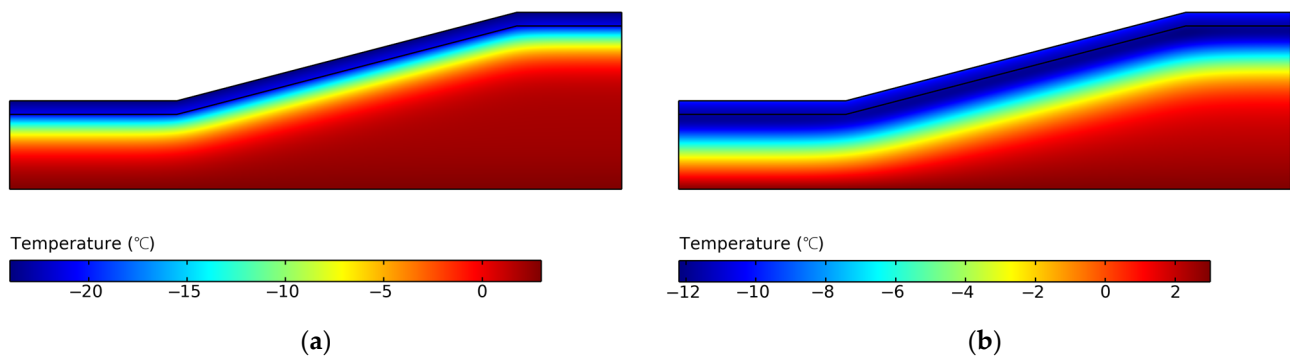
Figure 4. Temperature distributions of the canal at (**a**) 50 h and (**b**) 80 h.

As time progressed, the temperature gradient caused by negative temperature gradually decreased. Since the lower boundary temperature of the canal was a constant temperature of 3 °C, when the temperature drop caused by the negative temperature and the temperature rise caused by the lower boundary could cancel each other, the negative temperature will no longer develop downward. Figure 5 shows the temperature distribution of the canal at that time (97 h).
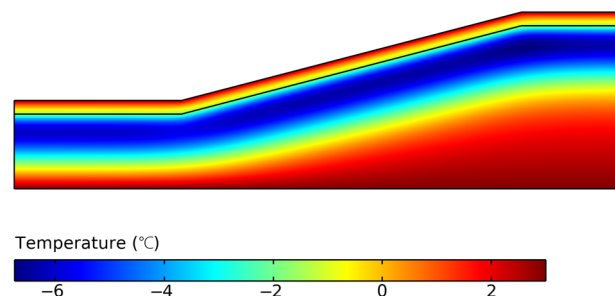

Figure 5. Temperature distributions of the canal at 97 h.

With the temperature increase of the upper surface, the heat transferred from the upper boundary and lower boundary to the middle of the canal, and the temperature of the canal increased continuously. Figure 6 shows the temperature distributions of the canal at the calculation time of 110 h and 146 h. It can be seen that the temperature of the soil increased in a bidirectional trend.
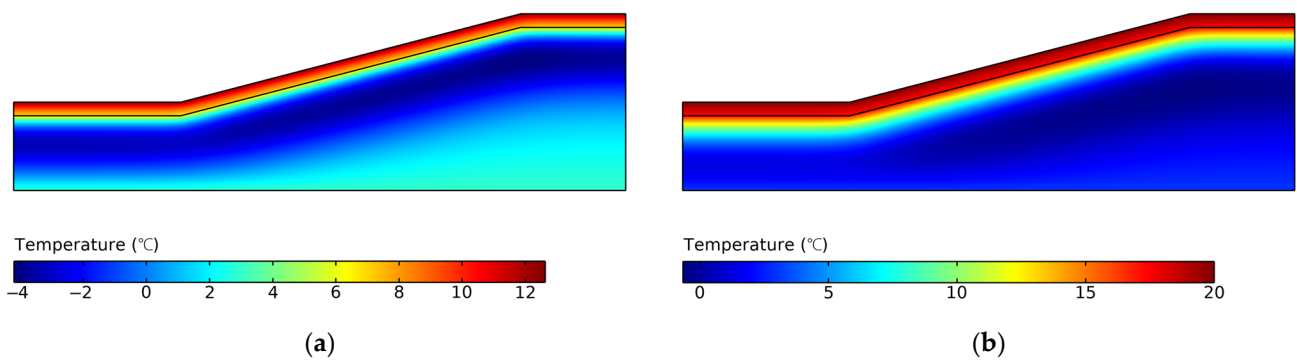
Figure 6. Temperature distributions of the canal at (**a**) 110 h and (**b**) 146 h.

4.2.2. Evolution of ice Content and Frost Depth

The water began to freeze when the temperature of the soil was lower than its freezing point. It can be known from the evolution of the canal temperature distribution that within the calculation time of 0~97 h, the negative temperature of the canal gradually developed downward, and the water in the soil froze continuously. The ice content distributions of the soil at the calculation time of 20 h and 80 h are given in Figure 7. The results showed that the freezing process of the soil was unidirectional, and the frozen surface was nearly parallel to the upper boundary of the canal. The freezing characteristic of the soil was consistent with the distribution and evolution characteristics of temperature and experimental results.
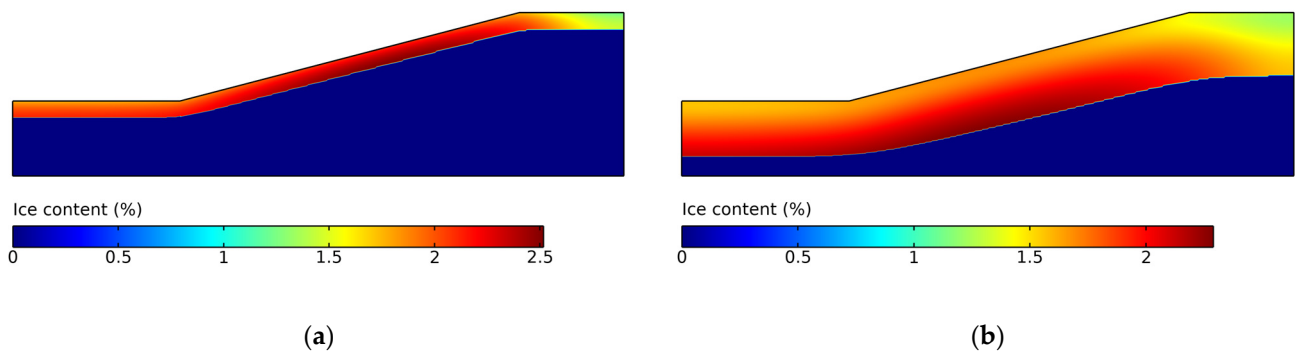

Figure 7. Ice content distribution of the soil at (**a**) 20 h and (**b**) 80 h.

The frost depth of the soil reached the maximum value at the calculation time of 97 h, which was consistent with the evolution of temperature distribution. Figure 8 shows the ice content distribution of the canal at 97 h. The frost depth was defined as the vertical distance from the upper surface of the soil contact with the concrete lining to the lowest frozen surface.
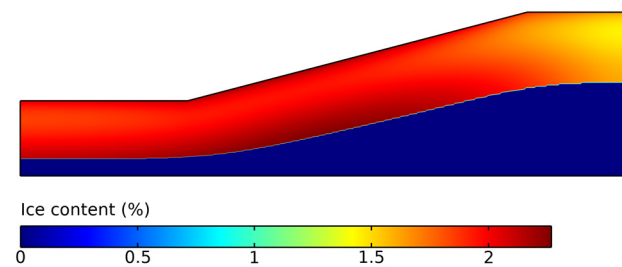

Figure 8. Ice content distribution of the soil at 97 h.

When the calculation time exceeded 97 h, the heat transferred from the upper and lower boundaries to the middle, and the ice in the soil began to melt. The ice content distributions of the canal at the calculation time of 110 h and 120 h are given in Figure 9. It can be seen that the thawing process of the soil was bidirectional. The evolution characteristic of the thawing process of the soil obtained in this paper was in line with the experimental results.
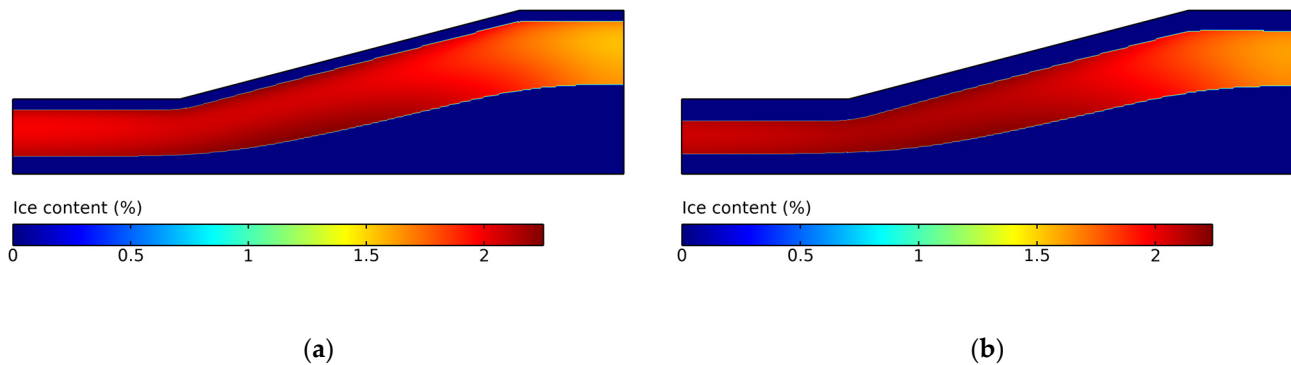

(**a**)　　　　　　　　　　　　　　　　　　　　　　　　　　　　　(**b**)

Figure 9. Ice content distribution of the soil at (**a**) 110 h and (**b**) 120 h.

Figure 10 shows the time-history curves of the frost depth of the soil foundation obtained from the calculation and indoor test. It can be seen that the evolution of the calculated frost depth was in good agreement with the experimental results. At the calculation time of 97 h, the frost depth of the soil foundation reached the maximum value. The calculated maximum frost depth was about 47.2 cm, which was slightly larger than the measured value of the test, approximately 44.94 cm.
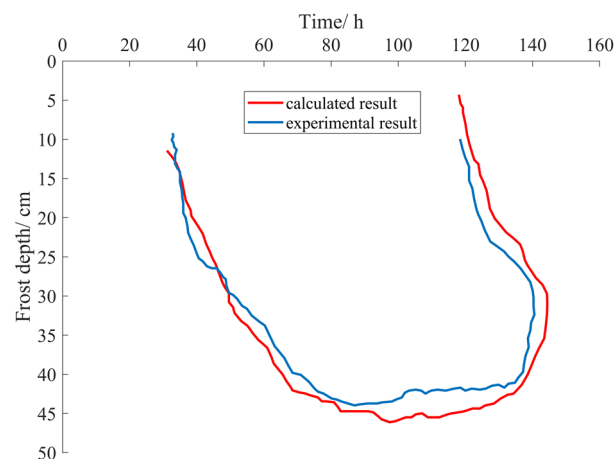

Figure 10. Time-history curves of the frost depth.

4.2.3. Evolution of Frost heave Deformation

Figure 11 shows the time-history curves of the frost heave deformation of the soil foundation at the top of the canal obtained from the calculation and indoor test. It can be seen that the frost heave deformation results obtained by calculation were consistent with the experimental results. The calculated maximum frost heave deformation was about 23.97 mm, slightly larger than the measured value of the experiment, approximately 22.41 mm.

According to the calculated time-history curve of the frost heave deformation of the soil foundation under the given external temperature conditions, the frost heave deformation can be divided into four stages: ① Compression deformation stage. Within the calculation time of 0~8 h, the freezing of pore water in the concrete caused the frost heave deformation of the lining, and the soil foundation was compressed and deformed downward. Therefore,

the frost heave deformation of the soil foundation within 0~8 h was negative, consistent with the phenomenon obtained from the experiment; ② Rapid development stage. Within the calculation time of 8 h~76 h, the soil temperature gradually decreased, the pore water in the soil began to freeze, and the frost heave deformation of the soil foundation increased rapidly; ③ Slow development stage. Within the calculation time of 76~97 h, the temperature gradient caused by negative temperature decreased, and the freezing rate of pore water in the soil slowed down. The growth rate of frost heave deformation decreased, and the frost heave deformation of the soil foundation reached the maximum value in 97 h; ④ Rapid dissipation stage. Within the calculation time of 97~160 h, the soil temperature gradually rose, the ice in the soil melted from the inside to the surface and bottom, and the frost heave deformation of the soil foundation dissipated rapidly.

The time-history curves of the frost heave deformation at different positions of the soil foundation are shown in Figure 12. It can be seen that the frost heave deformation values at different positions of the soil foundation were different. At the calculation time of 97 h, the frost heave deformation at different soil foundation positions reached the maximum value in the order of 1/2 slope height > 1/3 slope height > 1/4 slope height > 1/7 slope height > the top of the canal > the bottom of the canal, which was consistent with the experimental results. The frost heave deformation of the soil foundation at the 1/2~1/3 slope height area was the largest, which can easily lead to cracking and damage to the concrete lining in this area.
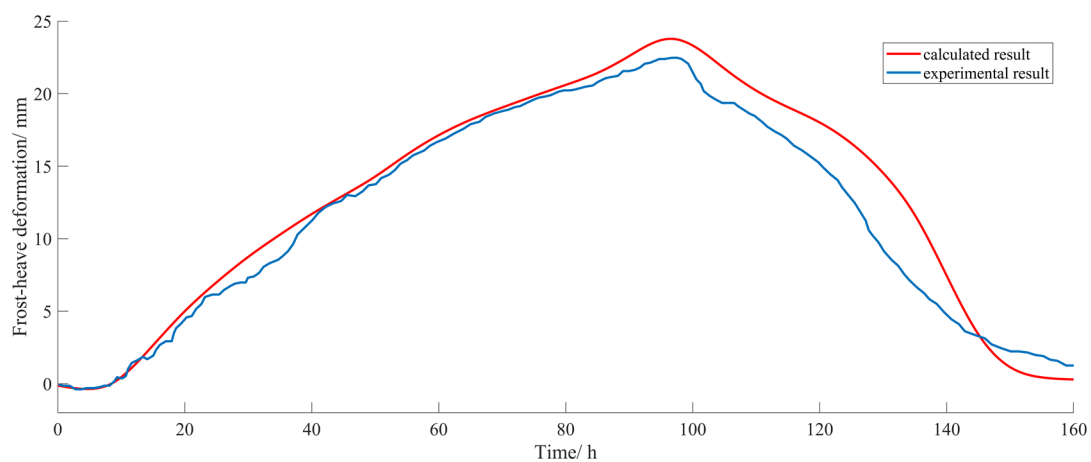

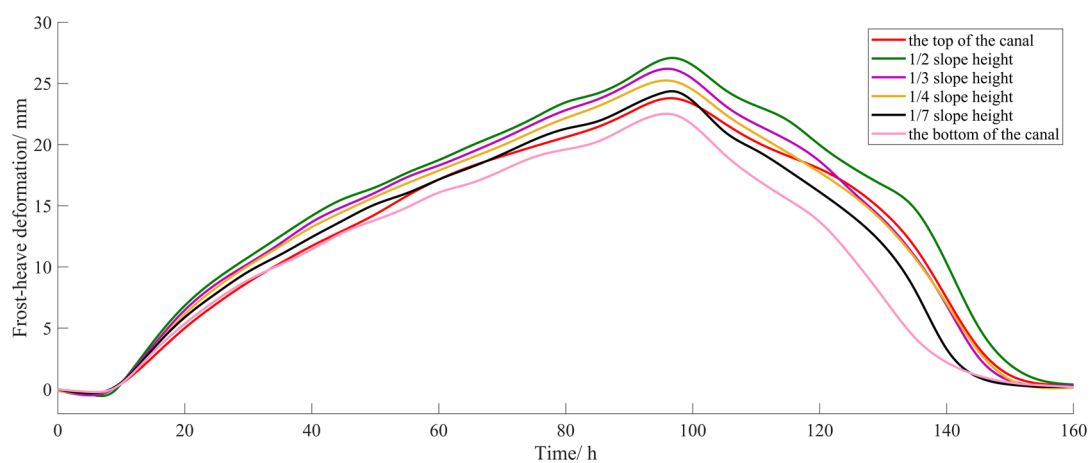**Figure 11.** Time-history curves of the frost heave deformation at the top of the canal.

Figure 12. Time-history curves of the frost heave deformation at different positions.

5. Conclusions

Regarding concrete as a porous medium, a thermal-hydro-mechanical coupling analysis model for concrete-lined canals under freeze–thaw conditions is established, in which the effects of the pore structure of concrete, the water content, ice content, and ice-water phase transition are taken into account. The temperature distribution, frost depth development, and frost heave deformation of the canal during the freeze–thaw process are calculated, which agrees with the experimental results. The proposed model can effectively predict the frost heave deformation of the concrete-lined canals and provide a reference for the design and disaster prevention of concrete-lined canals in cold regions.

The distribution characteristics of the frost heave deformation of a canal are affected by many factors. When the external temperature decreases first and then increases, the frost heave deformation of the soil foundation of the canal can be divided into four stages, i.e., the compression deformation stage, the rapid development stage, the slow development stage, and the rapid dissipation stage. The frost heave deformation of the soil foundation at the 1/2~1/3 slope height area is the largest, and the concrete lining is more prone to cracking and damage in this area.

The subsequent research can further consider the failure characteristics of concrete, study the cracking of concrete lining under a freeze–thaw environment, analyze the development of cracks based on concrete pore structure, and put forward corresponding prevention and control measures. In addition, the freeze–thaw problem of the canal under normal water transport conditions can be studied, and the influence of ice cover on the frost heave deformation of the canal can be modeled as well. Research on the above issues is in progress.

Author Contributions: Conceptualization, Q.Z.; formal analysis, R.T.; funding acquisition, Q.Z.; writing—original draft preparation, R.T.; methodology, R.T. and Q.Z.; writing—review and editing, X.G. and X.X. All authors have read and agreed to the published version of the manuscript.

Data Availability Statement: Related data are available upon reasonable request.

Conflicts of Interest: The authors declare no conflict of interest.

References

1. Kong, L.Z.; Quan, J.; Yang, Q.; Song, P.B.; Zhu, J. Automatic control of the middle route project for south-to-north water transfer based on linear model predictive control algorithm. *Water* **2019**, *11*, 1873. [CrossRef]
2. Grigg, N. Large-scale water development in the United States: TVA and the California State Water Project. *Int. J. Water Resour. Dev.* **2021**, *39*, 70–88. [CrossRef]
3. Li, S.Y.; Lai, Y.M.; Zhang, M.Y.; Pei, W.S.; Zhang, C.; Yu, F. Centrifuge and numerical modeling of the frost heave mechanism of a cold-region canal. *Acta Geotech.* **2019**, *14*, 1113–1128. [CrossRef]
4. Li, S.Y.; Zhang, M.Y.; Tian, Y.B.; Pei, W.S.; Zhong, H. Experimental and numerical investigations on frost damage mechanism of a canal in cold regions. *Cold Reg. Sci. Technol.* **2015**, *116*, 1–11. [CrossRef]
5. Taber, S. The mechanics of frost heaving. *J. Geol.* **1930**, *38*, 303–317. [CrossRef]
6. Everett, D.H. The thermodynamics of frost damage to porous solids. *Trans. Faraday Soc.* **1961**, *57*, 1541–1551. [CrossRef]
7. Miller, R.D. Freezing and heaving of saturated and unsaturated soil. *Highw. Res. Rec.* **1972**, *393*, 1–11.
8. O'Neill, K.; Miller, R.D. Exploration of a rigid ice model of frost heave. *Water Resour. Res.* **1985**, *21*, 281–296. [CrossRef]
9. Harlan, R.L. Analysis of coupled heat-fluid transport in partially frozen soil. *Water Resour. Res.* **1973**, *9*, 1314–1323. [CrossRef]
10. Mo, T.F.; Lou, Z.K. Numerical simulation of frost heave of concrete lining trapezoidal channel under an open system. *Water* **2020**, *12*, 335. [CrossRef]
11. Liu, Y.; Wang, Z.Z.; Wang, Y.; Liu, Q.H.; Guo, R.; Xiao, M. Frost heave model of canal considering influence of moisture migration and phase transformation on temperature field. *Trans. Chin. Soc. Agric. Eng.* **2016**, *32*, 83–88. [CrossRef]
12. Wang, Z.Z.; Liu, S.J.; Wang, Y.; Liu, Q.H.; Ge, J.R. Size effect on frost heave damage for lining trapezoidal canal with arc-bottom in cold regions. *J. Hydraul. Eng.* **2018**, *49*, 803–813. [CrossRef]
13. Shang, H.S.; Song, Y.P. Experimental study of strength and deformation of plain concrete under biaxial compression after freezing and thawing cycles. *Cem. Concr. Res.* **2006**, *36*, 1857–1864. [CrossRef]

14. Liu, D.Y.; Tu, Y.M.; Sas, G.; Elfgren, L. Freeze-thaw damage evaluation and model creation for concrete exposed to freeze-thaw cycles at early-age. *Constr. Build. Mater.* **2021**, *312*, 125352. [CrossRef]

15. Qiu, W.L.; Peng, R.X.; Jiang, M. Meso equivalent calculation model for frost evaluation of concrete. *Constr. Build. Mater.* **2021**, *272*, 121867. [CrossRef]

16. Tahiri, I.; Dangla, P.; Vandamme, M.; Vu, Q. Numerical investigation of salt-frost damage of pervious concrete at the scale of a few aggregates. *Cem. Concr. Res.* **2022**, *162*, 106971. [CrossRef]

17. Coussy, O.; Monteiro, P. Poroelastic model for concrete exposed to freezing temperatures. *Cem. Concr. Res.* **2008**, *38*, 40–48. [CrossRef]

18. Wang, Z.D.; Zeng, Q.; Wang, L.; Li, K.F.; Xu, S.L.; Yao, Y. Characterizing frost damages of concrete with flatbed scanner. *Constr. Build. Mater.* **2016**, *102*, 872–883. [CrossRef]

19. Gong, F.Y.; Maekawa, K. Proposal of poro-mechanical coupling among ASR, corrosion and frost action for damage assessment of structural concrete with water. *Eng. Struct.* **2019**, *188*, 418–429. [CrossRef]

20. Peng, R.X.; Qiu, W.L.; Jiang, M. Frost resistance performance assessment of concrete structures under multi-factor coupling in cold offshore environment. *Build. Environ.* **2022**, *226*, 109733. [CrossRef]

21. Powers, T.C. A working hypothesis for further studies of frost resistance of concrete. *J. Am. Concr. Inst.* **1945**, *16*, 245–272. [CrossRef]

22. Coussy, O.; Dormieux, L.; Detournay, E. From mixture theory to Biot's approach for porous media. *Int. J. Solids Struct.* **1998**, *35*, 4619–4635. [CrossRef]

23. Coussy, O. Poromechanics of Freezing Materials. *J. Mech. Phys. Solids* **2005**, *53*, 1689–1718. [CrossRef]

24. Zuber, B.; Marchand, J. Modeling the deterioration of hydrated cement systems exposed to frost action: Part 1: Description of the mathematical model. *Cem. Concr. Res.* **2000**, *30*, 1929–1939. [CrossRef]

25. Zuber, B.; Marchand, J. Predicting the volume instability of hydrated cement systems upon freezing using poro-mechanics and local phase equilibria. *Mater. Struct.* **2004**, *37*, 257–270. [CrossRef]

26. Duan, A. Numerical simulation of the freezing process of concrete. *J. Mater. Civ. Eng.* **2013**, *25*, 1317–1325. [CrossRef]

27. Pan, C. Research of Damage Mechanism of Cement Concrete Pavement under Freezing Environment Based on FEM Numerical Simulation. Master's Thesis, Harbin Institute of Technology, Harbin, China, 2010.

28. Taylor, G.S.; Luthin, J.N. A model for coupled heat and moisture transfer during soil freezing. *Can. Geotech. J.* **1978**, *15*, 548–555. [CrossRef]

29. Jame, Y.W.; Norum, D.I. Heat and mass transfer in a freezing unsaturated porous medium. *Water Resour. Res.* **1980**, *16*, 811–819. [CrossRef]

30. Bai, Q.B.; Li, X.; Tian, Y.H.; Fang, J.H. Equations and numerical simulation for coupled water and heat transfer in frozen soil. *Chin. J. Geotech. Eng.* **2015**, *37*, 131–136. [CrossRef]

31. Tai, B.W.; Liu, J.K.; Li, X.; Yue, Z.; Shen, Y.P. Numerical model of frost heaving and anti-frost heave measures of high speed railway subgrade in cold region. *China Railw. Sci.* **2017**, *38*, 1–9. [CrossRef]

32. Liu, X.C. The Study of Frost Heaving Model on Water-Heat-Deformation Coupled Fields of Canal Slope in Seasonally Frozen Area. Master's Thesis, Northeast Agricultural University, Harbin, China, 2016.

33. Li, K.F.; Zeng, Q. Influence of freezing rate on cryo-damage of cementitious material. *J. Zhejiang Univ. Sci. A* **2009**, *10*, 17–21. [CrossRef]